Charge-dependent wavelength shifts and line intensities in the dielectronic satellite spectrum of heliumlike ions

TFR Group*
Association Euratom—Commissariat à l'Energie Atomique sur la Fusion, Département de Recherches sur la Fusion Contrôlée, Centre d'Etudes Nucléaires, Boîte Postale No. 6, 92260 Fontenay-aux-Roses, France

M. Cornille, J. Dubau, and M. Loulergue
Observatoire de Paris, 92190 Meudon, France
(Received 11 June 1985)

Wavelengths and atomic parameters for the satellite spectrum of the $1s^2$-$1s\,2p$ parent lines of heliumlike ions from Ar^{16+} to Mn^{23+} have been calculated using a multiconfiguration intermediate-coupling scheme with a statistical Thomas-Fermi potential. The results are compared to high-resolution x-ray spectra of Ar^{16+}, Sc^{19+}, V^{21+}, Cr^{22+}, and Mn^{23+} obtained from plasmas generated at the Tokamak de Fontenay-aux-Roses.

I. INTRODUCTION

The electron temperatures and particle confinement times in tokamak plasmas permit the ionization of heavy impurity elements up to the heliumlike (eventually hydrogenlike) charge state. High-resolution x-ray spectroscopy of the line emission of these ions has become a powerful technique for determining the electron and ion temperatures T_e and T_i, the macroscopic plasma movement, and the dynamics of plasma impurity transport.[1,2] Besides being important for these diagnostic applications to laboratory plasmas and for the corresponding extension to solar flares,[2,3] the x-ray spectra of heliumlike ions (from S^{14+} to Ni^{26+}) are of greatest interest for the theory of the high-charge, few-electron quantum system.

By means of Bragg crystal spectrometers, high-quality spectra for diagnostic-relevant impurities have been obtained from several large tokamaks: Ti^{20+} and Fe^{24+} from the Princeton Large Torus, Princeton University,[4,5] Cr^{22+} from the Tokamak de Fontenay-aux-Roses (TFR),[6] Ar^{16+} from TFR,[7] and the Alcator-*C*, Massachusetts Institute of Technology.[8] At TFR the particular layout of the crystal spectrometer [spectral range from about 1.5 to 5 Å (Ref. 9)] together with the technique of doping by laser evaporation[10] make the spectrometer a powerful device for fundamental spectroscopy.

We have now also observed the dielectronic satellite spectra of heliumlike scandium, vanadium, and manganese. Our observations for five elements from Ar^{16+} to Mn^{23+} represent the largest sequence of high-resolution spectra obtained on the same device under nearly identical plasma and instrumental conditions. In this paper we present a coherent set of atomic data (wavelengths and intensity factors) for the dielectronic satellite lines of heliumlike ions of interest in plasma physics. The results are compared to the TFR spectra of Ar, Sc, V, Cr, and Mn.

II. ATOMIC PHYSICS CALCULATIONS

The spectral lines we are concerned with in this paper are the characteristic lines w,x,y,z ($1s^2\,{}^1S_0 - 1s\,2p\,{}^1P_1, {}^3P_2, {}^3P_1$, $1s\,2s\,{}^3S_1$) of the heliumlike ion and the associated satellite lines of the type $1s^2 2l$-$1s\,2l\,2p$ produced by dielectronic recombination to, or inner-shell excitation of, the lithiumlike ion. For the calculation of the wavelengths and intensity-related atomic data we use a multiconfiguration intermediate-coupling scheme with a statistical Thomas-Fermi potential. Details of these calculations and the various excitation processes under real plasma conditions (including radiative cascades and inner-shell ionization) may be found elsewhere.[11,12] Here it is sufficient to specify that the results presented in this paper have been obtained in the same way for all elements. For each one the scaling parameters $\Lambda_s, \Lambda_p, \Lambda_d$ were adjusted through a minimization of the energy sum of all the terms belonging to the following configurations: $1s^2 2s$, $1s^2 3d$, $1s\,2s\,2p$, and $1s\,2p\,3d$ (Λ_f was set equal to Λ_d). The values of the scaling parameters are given in Table I. They have been used to calculate the atomic data (wavelengths, transition probabilities) in a more extended configuration basis which contains all the configurations $1s^2 nl$, $1s\,2l'nl$ with $n=2,3,4,5$, $l=0,1,2,3$, and $l'=0,1$.

The wavelengths of the most prominent heliumlike and satellite lines are given in Table II. Wavelength shifts normalized with respect to the resonance line w [i.e., $(\lambda-\lambda_w)/(\lambda_z-\lambda_w)$] are shown in Fig. 1. This plot makes quite apparent the charge-dependent line shifts, in particular the increasing separation between lines x and y with increasing Z. In the energy scale [i.e., $(\lambda_y-\lambda_x)\lambda_w^{-2}$] this separation increases by a factor of 4.2 between Ar and Mn, mainly due to the Z^4 dependence of the spin-orbit interaction energy (the Coulomb interaction energy and,

TABLE I. Thomas-Fermi scaling parameters used for the calculations.

	Ar	Sc	V	Cr	Mn
Λ_s	2.7328	2.7338	2.7350	2.7356	2.7360
Λ_p	2.1744	2.1747	2.1750	2.1750	2.1750
Λ_d	1.9404	1.9404	1.9404	1.9404	1.9404

 ©1985 The American Physical Society

TABLE II. Calculated wavelengths and satellite intensity factors. λ in Å, F_2^* in 10^{13} s^{-1}.

		Ar		Sc		V		Cr		Mn	
	Array	λ	F_2^*	λ	F_2^*	λ	F_2^*	λ	F_2^*	λ	F_2^*
w	$1s2p\ ^1P_1-1s^2\ ^1S_0$	3.9457		2.8697		2.3787		2.1789		2.0030	
x	$1s2p\ ^3P_2-1s^2\ ^1S_0$	3.9632		2.8803		2.3866		2.1857		2.0090	
s	$1s2s2p\ ^2P_{3/2}-1s^22s\ ^2S_{1/2}$	3.9648	1.79	2.8814	2.46	2.3876	2.56	2.1866	2.47	2.0098	2.27
t	$1s2s2p\ ^2P_{1/2}-1s^22s\ ^2S_{1/2}$	3.9660	3.34	2.8825	6.77	2.3885	8.96	2.1875	9.81	2.0107	10.45
m	$1s2p^2\ ^2S_{1/2}-1s^22p\ ^2P_{3/2}$	3.9629	2.58	2.8810	3.55	2.3876	4.15	2.1868	4.58	2.0102	4.72
y	$1s2p\ ^3P_1-1s^2\ ^1S_0$	3.9671		2.8843		2.3907		2.1899		2.0132	
q	$1s2s2p\ ^2P_{3/2}-1s^22p\ ^2S_{1/2}$	3.9784	0.97	2.8899	0.46	2.3939	0.19	2.1923	0.13	2.0148	0.01
k	$1s2p^2\ ^2D_{3/2}-1s^22p\ ^2P_{1/2}$	3.9875	16.61	2.8950	25.88	2.3975	30.80	2.1953	33.15	2.0173	34.23
r	$1s2s2p\ ^2P_{1/2}-1s^22s\ ^2S_{1/2}$	3.9808	2.70	2.8925	3.92	2.3968	4.87	2.1952	5.53	2.0179	5.86
a	$1s2p^2\ ^2P_{3/2}-1s^22p\ ^2P_{3/2}$	3.9831	3.43	2.8928	6.47	2.3961	8.75	2.1941	10.10	2.0164	11.02
j	$1s2p^2\ ^2D_{5/2}-1s^22p\ ^2P_{3/2}$	3.9917	22.88	2.8988	35.50	2.4010	43.27	2.1986	47.11	2.0205	49.46
z	$1s2s\ ^3S_1-1s^2\ ^1S_0$	3.9916		2.9000		2.4028		2.2006		2.0227	

consequently, the value of λ_w^{-1} scale with Z^2). The spin-orbit interaction is also responsible for the increasing $r-q$ and $j-k$ distances (in this context, the more spectacular separation of j from z is not of interest because the lines belong to different ions).

With respect to the intensities of the spectral lines, we first notice that the line q is mainly due to collisional excitation of the lithiumlike ion. Neglecting recombination and cascade effect for w, the ratio of the local emissivities of these lines is $\epsilon_q/\epsilon_w \approx \frac{2}{3} n_{\mathrm{Li}}/n_{\mathrm{He}}$, where n_{Li} and n_{He} are the densities of the Li- and He-like ions, respectively

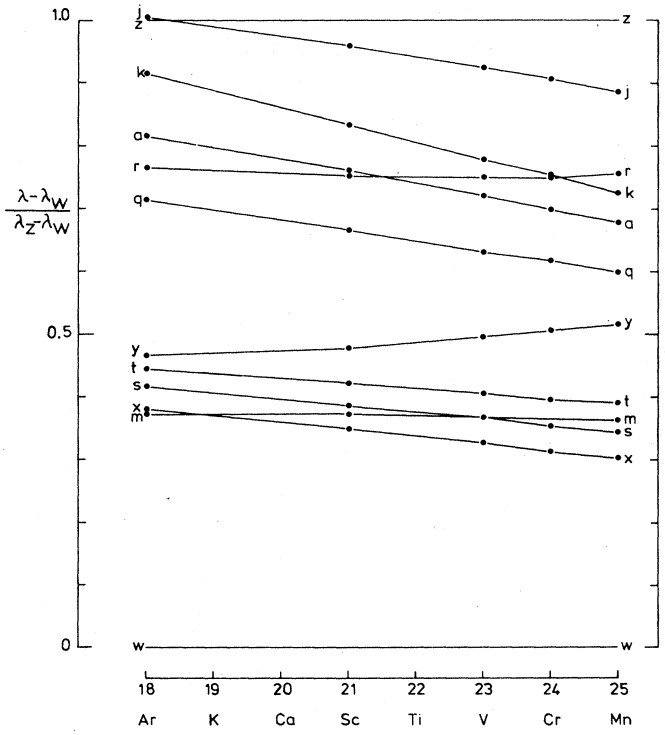

FIG. 1. Normalized wavelength shifts as function of nuclear charge.

(from optically thin plasmas the ratio of the line-of-sight integrated emissivities is observed). For a satellite (s) line which is excited mainly by dielectronic recombination from the He-like to the Li-like ion, we have [2,3]

$$\frac{\epsilon_s}{\epsilon_w} = \frac{F_1(s,T_e)F_2^*(s)}{C_w(T_e)} ,$$

$$F_1(s,T_e) = (1.65\times 10^{-22}) T_e^{-3/2} \exp(-E_s/T_e) ,$$

where E_s and T_e are in eV. $F_2^*(s)$ is a line-specific intensity factor given in Table II. $C_w(T_e)$ is the rate coefficient (in cm^3 s^{-1}) for collisional excitation of line w. E_s is the difference in energy of the satellite state in the recombined ion and the ground state in the recombining ion.[2,3]

The ϵ_s/ϵ_w ratio may be used as a diagnostic for the electron temperature (provided the electron velocity distribution is Maxwellian). The ϵ_s/ϵ_w ratio increases very rapidly with increasing nuclear charge Z, due mainly to the Z^4 dependence of the radiative transition probabilities, A_r, in the expression for $F_2^*(s)$. In this context it is instructive to make use of a Z-scaling law for the $C_w(T_e)$ of two elements A and B:[13,14]

$$C_w^A(T_e) = \gamma^3 C_w^B(\gamma^2 T_e) ,$$

where $\gamma = Z_B - 0.5)/(Z_A - 0.5)$.

Taking for C_w^B the calcium data of Ref. 11, a numerical evaluation for the most prominent satellite line j shows that $\epsilon_j/\epsilon_w \simeq Z^n$, where $n=7.1$ at $T_e=1550$ eV (n is very weakly T_e dependent between 1000 and 2000 eV).

III. EXPERIMENTS

The x-ray spectra have been observed by means of a Johann-type crystal spectrometer.[9] The diffracting crystals are interchangeable quartz plates ($50\times 30\times 0.4$ mm^3) in a vacuum mount (radius of curvature 288 cm). With the exception of the argon spectrum, all observations have been done with a new large-area, multianode-wire position-sensitive detector (window height 40 mm, window length 100 mm, i.e., exceeding the physical length of the spectra shown here). The experimental conditions

TABLE III. Instrumental and plasma-related data.

	Ar	Sc	V	Cr	Mn
Origin of the impurity	Valve injection	Laser evaporation	Laser evaporation	Natural	Laser evaporation
Crystal cut	$20\bar{2}0$	$21\bar{3}1$	$10\bar{1}4$	$31\bar{4}0$	$31\bar{4}2$
Crystal spacing $2d$ (Å)	4.256	3.082	2.576	2.3604	2.1632
Bragg angle at λ_w (in deg)	67.964	68.548	67.389	67.347	67.783
Detector conversion factor (channels/mm)	12.30	8.433	8.429	8.433	8.414
T_e (plasma center) (eV)	1250	1600	1550	1500	1550

(plasma, crystal, and detector data) are given in Table III. In particular, we note that the observations were done at almost identical Bragg angles, i.e., the instrumental resolution is the same in all cases ($\lambda/d\lambda \sim 15\,000$). Another important number is the conversion factor of the position-encoding x-ray detector (channels/mm). This factor has been measured after each experiment with a highly collimated x-ray source mounted on a precision translation stage. As seen from Table III, there is very little drift of the conversion factor (besides a deliberate change for the argon experiment), i.e., the dispersion of the crystal spectrometer is accurately known (to better than 0.2%). Finally, we notice that four elements (Sc to Mn) have been observed under almost identical plasma conditions (electron temperature $T_e = 1550 \pm 50$ eV, Thomson scattering).

Figure 2 shows the observed spectra of Ar, Sc, V, Cr, and Mn. Each of the five subfigures has two abscissas. One abscissa is the original data-acquisition-system scale (50 channels/division), the other is the true (slightly nonlinear) wavelength scale, calculated from the Bragg condition, taking for λ_w the value given in Table II. We have also indicated the calculated position of the other lines (from Table II). The line labeled 1 in the manganese spectrum is the $1s^2 2s^2\,{}^1S_0 - 1s\,2s^2 2p\,{}^1P_1$ dielectronic satellite line from the Be-like ion (this line does not appear in the other spectra due to a vignetting effect of the tokamak viewing port).

IV. COMPARISON OF THEORY AND EXPERIMENT

The charge-dependent line shifts mentioned above are very clearly illustrated in Fig. 2, in particular the increasing separation of lines x and y and the progressive separation of the diagnostically important line j from line z. Another striking feature is the position of the $n=3$ satellite group. Well separated from the resonance line w and from higher-order satellites in the case of argon, the group gradually shifts towards the line and is partially integrated into its long-wavelength wing. This effect is also predicted by theory (analytically this is seen in the Z-expansion method).

The comparison of observed and calculated wavelengths is restricted here to the comparison of shifts from the resonance line w (we have not observed standard lines in our spectra which would permit absolute wavelength calibration, but the dispersion of the instrument is always well known). The observed values of $\lambda - \lambda_w$ are listed in Table IV for all five elements. For well-isolated lines, the values are quite accurate (uncertainty of 10–20% of the Doppler width); in case of blending the center of gravity is given. The comparison with theoretical spectra has been done by calculating for each line the "double difference" $d\lambda$:

$$d\lambda = (\lambda - \lambda_w)_{\text{theory}} - (\lambda - \lambda_w)_{\text{expt}} .$$

We have done this for two sets of theoretical data, (1) the present work, Table II, and (2) Vainshtein and Safronova.[15] The mean values $\langle d\lambda \rangle_1$ and $\langle d\lambda \rangle_2$ are given in the last two rows of Table IV. We notice that the two methods for calculating theoretical wavelengths, i.e., the statistical Thomas-Fermi approach and the $1/Z$-expansion method, are both quite adequate for Sc, V, Cr, and Mn. For argon, however, the value of $\langle d\lambda \rangle_1 = 0.9$ is obviously beyond the experimental uncertainties, in contrast to $\langle d\lambda \rangle_2$. In fact, this was expected, since Vainshtein and Safronova have included all bound states and continua in their perturbation treatment. Their wavelength values are therefore, in principle, more accurate than ours, especially at lower values of the nuclear charge. (Finally, we mention the multiline synthetic-spectrum technique[12] as an alternative approach for a quantitative

TABLE IV. Observed wavelength shifts $\lambda - \lambda_w$ in mÅ for lines from x to z. Averaged deviation from theoretical values (last two rows; see text for explanation).

	Ar	Sc	V	Cr	Mn
x	16.6	10.3	7.8	6.7	5.6
t			9.7	8.3	7.4
y	20.2	14.0	11.8	10.6	9.9
q	32.2	20.2	15.4	13.4	12.0
a	36.4	22.7	18.5	16.2	14.5
r	34.2				
k	40.9	25.1			
j	45.0	29.2	22.3	19.6	17.6
z			24.0	21.5	19.6
$\langle d\lambda \rangle_1$	0.9	0.3	−0.1	0.1	0.1
$\langle d\lambda \rangle_2$	0.2	−0.1	−0.3	−0.1	−0.1

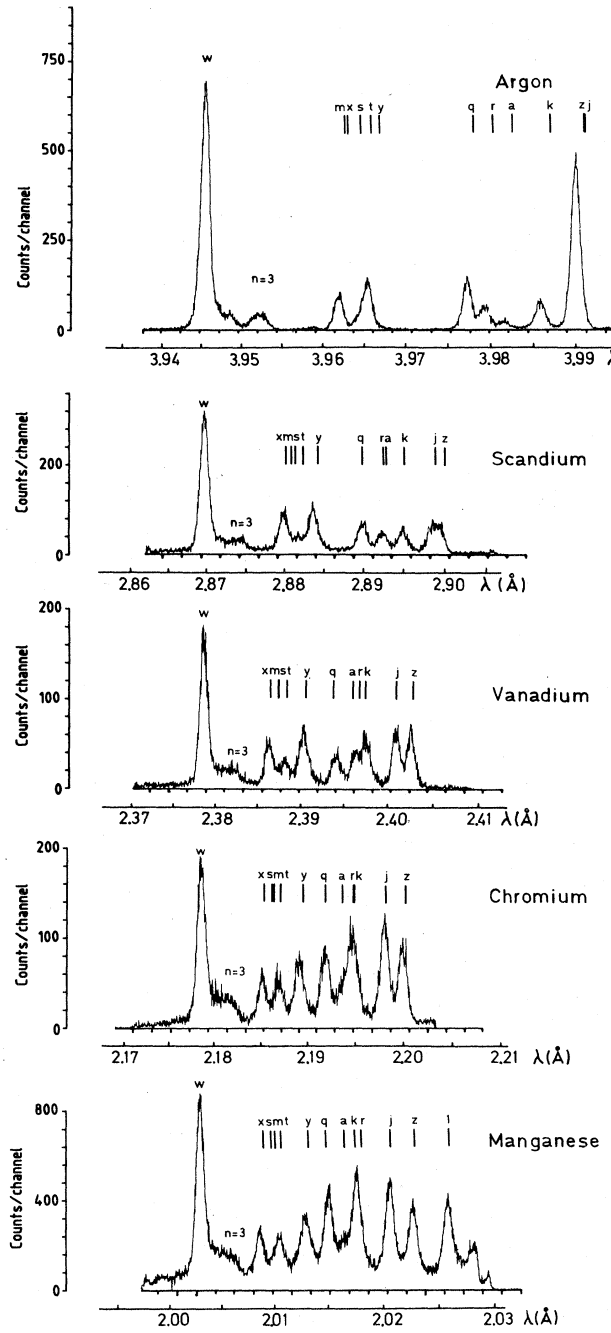

FIG. 2. Experimental x-ray spectra from TFR.

comparison of theory and experiment. However, this would be beyond the scope of the present work.)

With respect to the line intensities (relative to w) we concentrate on the four elements from Sc to Mn observed under nearly identical plasma conditions (T_e, Table III). The increase of the dielectronic satellite lines (j, t) with increasing charge Z is quite obvious. As mentioned before, an increase by a factor of $(Z_{\mathrm{Mn}}/Z_{\mathrm{Sc}})^{7.1}=3.45$ is expected for the j-w line-intensity ratio at $T_e=1550$ eV. The observations are compatible with this factor. In fact, from a rough inspection of the Sc and Mn spectra we calculate a factor of 3.5 ± 0.8 (a more quantitative evaluation may be obtained by means of the multiline fitting program using synthetic spectra[12]). There is also an important increase of the q-w line-intensity ratio with increasing Z. This is due to the fact that, under identical plasma conditions, elements with higher values of Z are less ionized. It is also evident from the observed spectra that the z-$(x+y)$ intensity ratio increases between Sc and Mn, i.e., there is an apparent increase with nuclear charge Z at constant electron temperature. Collisional excitation from the heliumlike ground state would lead to a decrease of this inten-

sity ratio with Z (T_e=const). The surplus intensity of the z line is due to excitation of the $1s2s\,^3S_1$ level by inner-shell ionization of the lithiumlike ground state. The relative contribution from this process to the total line intensity increases with increasing $n_{\mathrm{Li}}/n_{\mathrm{He}}$, i.e., increasing Z at T_e=const.

V. CONCLUSION

We have reported on the dielectronic satellite spectra of the heliumlike ions Ar^{16+}, Sc^{19+}, V^{21+}, Cr^{22+}, and Mn^{23+} in the x-ray domain (λ=2–4 Å). Calculated atomic data (wavelengths, intensity factors) and spectra observed from TFR tokamak plasmas have been presented. Calculated and observed line positions agree to better than 0.001 Å. In particular, the effect of the nuclear-charge-dependent spin-orbit interaction is confirmed by the experiment. We have also observed the sharp increase of the intensity of dielectronic-recombination lines (relative to the resonance line) with increasing nuclear charge. Finally, anomalous intensities of the heliumlike forbidden line z are assigned to inner-shell ionization of the lithiumlike ground state.

*M. H. Achard, J. Adam, J. Andreoletti, P. Bannelier, H. Barkley, J. F. Bonnal, C. Breton, J. Breton, R. Brugnetti, J. L. Bruneau, M. Calderon, R. Cano, H. Capes, M. Charet, M. Chatelier, A. Cohen, M. Cotsaftis, J. P. Crenn, B. De Gentile, C. De Michelis, H. W. Drawin, J. Druaux, M. Dubois, J. L. Duranceau, A. Fissolo, M. Fois, D. Gambier, A. Geraud, F. Gervais, P. Giovannoni, A. Grosman, W. Hecq, T. Hutter, L. Jacquet, J. Johner, H. Kuus, J. Lasalle, L. Laurent, O. Lazare, P. Lecoustey, F. Linet, G. Martin, E. Maschke, M. Mattioli, R. Oberson, J. Olivain, M. Pain, P. Platz, A. L. Pecquet, L. Pignol, A. Quemeneur, J. Ramette, L. Rebuffi, C. Reverdin, J. P. Roubin, A. Samain, B. Saoutic, F. Simonet, R. Soubaras, J. Tachon, J. Touche, B. Tournesac, D. Veron, and B. Zanfagna.

[1]S. von Goeler, M. Bitter, S. Cohen, D. Eames, K. W. Hill, D. Hills, R. Hulse, G. Lenner, D. Manos, P. Roney, W. Roney, N. Sauthoff, S. Sesnic, W. Stodiek, F. Tenney, and J. Timberlake, in *Proceedings of the Course on Diagnostics for Fusion Reactor Conditions, Varenna, Italy, 1982,* edited by P. E. Stott *et al.* (Commission of the European Communities, Brussels, 1983), Vol. I, p. 109.

[2]A. H. Gabriel, Mon. Not. R. Astron. Soc. **160**, 99 (1972).

[3]J. Dubau and S. Volonte, Rep. Prog. Phys. **43**, 199 (1980).

[4]F. Bely-Dubau, P. Faucher, L. Steenman-Clark, M. Bitter, S. von Goeler, K. W. Hill, C. Camhy-Val, and J. Dubau, Phys. Rev. A **26**, 3459 (1982).

[5]M. Bitter, K. W. Hill, N. R. Sauthoff, P. C. Efthimion, E. Meservey, W. Roney, S. von Goeler, R. Horton, M. Goldman, and W. Stodiek, Phys. Rev. Lett. **43**, 129 (1979).

[6]TFR Group, J. Dubau, and M. Loulergue, J. Phys. B **15**, 1007 (1981).

[7]TFR Group and F. Bombarda, in *Proceedings of the 11th European Conference on Controlled Fusion and Plasma Physics, Aachen, FRG, 1983,* edited by S. Methfessel (European Physical Society, Aachen, 1983), Vol. I, p. 89.

[8]E. Källne, J. Källne, A. Dalgarno, E. S. Marmar, J. E. Rice, and A. K. Pradhan, Phys. Rev. Lett. **52**, 2245 (1984).

[9]P. Platz, J. Ramette, E. Belin, C. Bonnelle, and A. Gabriel, J. Phys. E **14**, 448 (1981).

[10]TFR Group, Phys. Lett. **87A**, 169 (1982).

[11]F. Bely-Dubau, J. Dubau, P. Faucher, A. H. Gabriel, M. Loulergue, L. Steenman-Clark, S. Volonte, E. Antonucci, and C. G. Rapley, Mon. Not. R. Astron. Soc. **201**, 1155 (1982).

[12]TFR Group, F. Bombarda, F. Bely-Dubau, P. Faucher, M. Cornille, J. Dubau, and M. Loulergue, Phys. Rev. A **32**, 2374 (1985).

[13]R. Mewe, J. Schrijver, and J. Sylvester, Astron. Astrophys. **87**, 55 (1980).

[14]R. Mewe, J. Schrijver, and J. Sylvester, Astron. Astrophys. Suppl. Ser. **40**, 323 (1980).

[15]L. A. Vainshtein and U. I. Safronova, At. Data Nucl. Data Tables **21**, 49 (1978).